ADVANCED SUSTAINABLE SYSTEMS
www.advsustainsys.com

Effect of the Substrate Materials in the Fabrication of an Electrode Based on Mixed Nickel-Iron Oxide Electrocatalyst

Yuuri Tsuji, Andrea Fiorani, and Yasuaki Einaga**

The effect of different substrate materials in the fabrication of an electrode intended for use in the water oxidation reaction is investigated. The electrocatalyst is nickel-iron oxide (NiFeOx) which is deposited by chronoamperometry on nickel, iron, titanium, and stainless steel substrates. The process of electrodeposition is optimized to achieve the lowest overpotential for the water oxidation reaction. The four electrodes are characterized by scanning electron microscopy (SEM), X-ray photoelectron spectroscopy (XPS), and glow-discharge optical emission spectroscopy (GDOES) to describe the effect of the substrate on the nature of the electrocatalyst layer. Electrochemical tests in 1 M NaOH are applied on the four electrodes to assess the stability and the retention of the electrocatalytic properties of the whole electrode. All electrodes show similar overpotential of ≈0.3 V at 10 mA cm^{-2} implying that the substrate do not affect the electrocatalytic activity of the NiFeOx. After use, the overpotential increases in a range of 30–50 mV for nickel, iron, and titanium substrates, while stainless steel retains the lowest overpotential with an increase of 10 mV. This limited variation can be the effect of smaller NiFeOx nanoparticles compared to other substrates. XPS analysis reveals that after galvanostatic electrolysis, the oxidation state of Fe shifts slightly from Fe(II) to Fe(III), likely Fe_3O_4 and Fe_2O_3, while NiO/Ni_2O_3 change partially to $Ni(OH)_2$.

1. Introduction

Electrochemical reactions are highly regarded as alternative to energy intensive processes as they can operate in mild conditions of temperature and pressure for the production of useful compounds to advance sustainable development. Beside the established industrial processes, such as adiponitrile synthesis or "Baizer process",[1] and chlor-alkali process,[2] promising applications include hydrogen from water electrolysis,[3] carbon dioxide reduction to hydrocarbons or oxygenates,[4] and nitrogen/nitrate reduction to ammonia.[5,6] Not limited to commodities, nowadays electrochemical synthesis is prospected to play an important role in the preparation of fine chemicals.[7,8]

The working electrode is generally regarded as worth the optimization for the reaction of interest, however, in an electrolytic cell, also the counter electrode should receive the same attention.[9] This was excellently shown in the industrial development of the Baizer process,[10] or for CO_2 reduction.[11]

The water oxidation reaction (WOR) is one of the most common counter electrode reactions, making the oxygen evolution reaction (OER) one of the most investigated electrochemical reactions[12] therefore, it also constitutes a perfect benchmark for development and optimization of electrodes.

The tendency to shift from noble metal oxides (Ru, Ir, and Pt)[13,14] to less precious and more abundant transition metals (Mn, Fe, Co, and Ni) leads to plenty of electrocatalysts available.[15–17]

Mixed nickel and iron oxides (NiFeOx) emerged as a valid alternative from the point of view of overpotential for OER in alkaline conditions[18–20] leading to a wide range of investigations on the WOR mechanism mediated by NiFeOx electrocatalyst.[21–24]

Generally, NiFeOx is not a free standing electrode per se, but it is deposited on a substrate that acts both as scaffold and current collector, same as for the most notable dimensionally stable anodes (DSA).[25–27]

Therefore, the substrate plays an important role in the final electrode properties which has been recognized for noble metal coated anodes.[28–30]

Focusing on the mechanistic understanding of the low overpotential at NiFeOx, the effect of the substrate has been largely overlooked, where carbon-based supports have been generally employed (glassy carbon and carbon fiber), or pure nickel.[31] Recently, the effect of substrate has attracted interest and been investigated for Au(111) and highly oriented pyrolytic graphite,[32] stainless steel,[33] or copper.[34]

In this research, we focused on NiFeOx as an electrocatalyst deposited on different metal substrates, such as nickel, iron, titanium and stainless steel (SUS302). Ni and Fe are the constituent

Y. Tsuji, A. Fiorani, Y. Einaga
Department of Chemistry
Keio University
3-14-1 Hiyoshi, Yokohama 223–8522, Japan
E-mail: andrea.fiorani@keio.jp; einaga@chem.keio.ac.jp

The ORCID identification number(s) for the author(s) of this article can be found under https://doi.org/10.1002/adsu.202300475

DOI: 10.1002/adsu.202300475

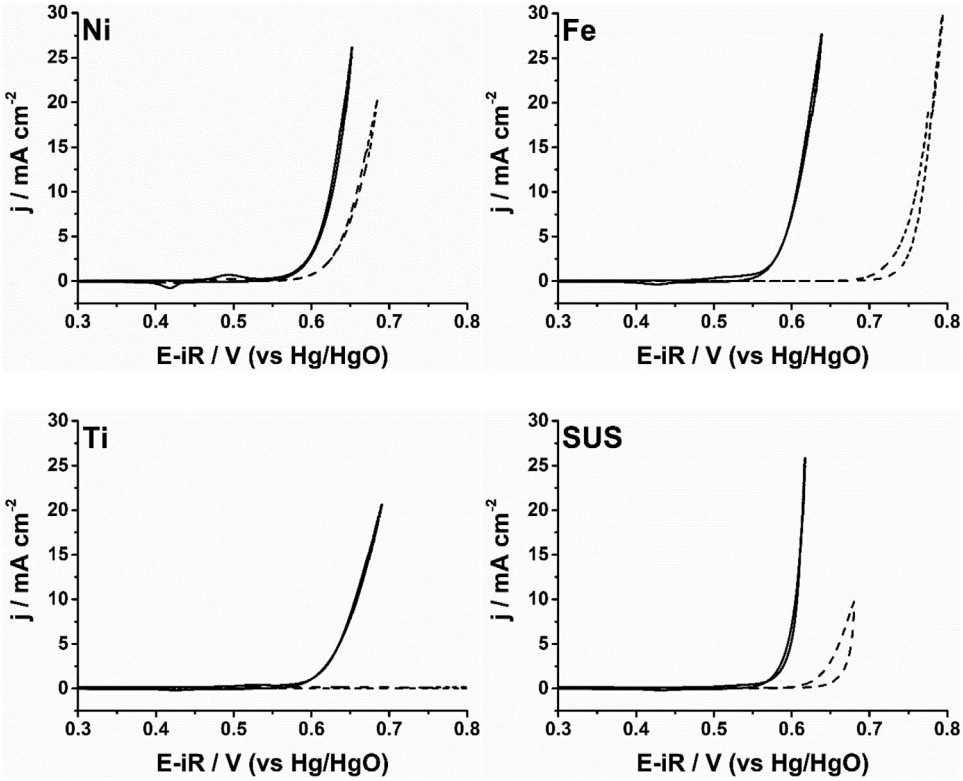

Figure 1. Ciclic voltammetry of NiFeOx deposited on Ni, Fe, Ti, and SUS in 1 M NaOH. Scan rate: 10 mV s^{-1}. Ohmic drop corrected.

of the catalyst, therefore the first option, also in term of expected adhesion of the catalyst being the same material. Titanium is the metal of choice as substrate for DSA electrode,[25,35] and stainless steel already finds technological application as electrode material.[1,36]

We assess the overpotential for the water oxidation reaction and the stability of the electrodes, substrate and electrocatalyst, to find which substrate will be more suitable in the fabrication of electrodes based on the NiFeOx.

2. Results and Discussion

The NiFeOx has already been established as a good electrocatalyst for the OER, and by this investigation, we want to assess the possibility to fabricate an electrode based on NiFeOx that can be used in practical applications. With an overpotential as low as 0.35 V,[17] the first optimization was to prepare an electrocatalysis with a comparable state-of-the-art overpotential. This was obtained by optimization of potential and time of electrodeposition (Figures S1–S3 and Table S1, Supporting Information). The overpotentials are very similar and increasing in the order (Fe) 324 mV ≈ (SUS) 325 mV < (Ni) 342 mV < (Ti) 374 mV (**Figure 1**).

To assess the quality of the NiFeOx, the Tafel slope has been measured by quasi steady-state polarization (**Figure 2**; Figures S4–S6 and Table S2, Supporting Information). The Tafel slope ranges from 30 to 45 mV dec^{-1}, in line with previous observations. This has been linked by a reaction pathway where an initial reversible discharge of hydroxyl ion is followed by a rate-limiting step with the formation of a hydrogen peroxide intermediate[22] which follows the reaction mechanism for water oxidation in alkaline solution.[37,38] Reasonably, the effect of the Fe is to provide a more favorable sites for the adsorption of the oxygen radical intermediate species.[18] Furthermore, a concerted reaction mechanism involving of Fe^{IV} and Ni^{III} intermediates has also been suggested.[23]

The electrodeposition shows a homogeneous layer of NiFeOx nanoparticles of different dimensions in the range of hundreds of nanometers: (Fe) 105 ± 28 nm ≈ (SUS) 117 ± 17 nm < (Ti) 225 ± 38 nm ≈ (Ni) 243 ± 77 nm (**Figures 3** and **4**).

The NiFeOx nanoparticles size follows the overpotential trend suggesting that smaller nanoparticle and more homogeneous surfaces might be beneficial to reduce the overpotential.

The NiFeOx thickness was estimated in the μm range (Figure S7, Supporting Information), and it is positively correlated with the charge used for the electrodeposition (Figure 4).

The NiFeOx composition was analyzed by glow-discharge optical emission spectroscopy to map the depth profile of Ni and Fe (Figure S8, Supporting Information). Generally, Ni is deposited in larger amount compared to Fe, although a 1:1 ratio is used in the plating solution. In particular, this is observed for Ni and Ti, where the amount of Ni is constantly higher than the amount of Fe. On the other hand, Fe and SUS show a less remarkable Ni amount which might be promoted by facilitated deposition of Fe by metal affinity. However, an optimized deposition of NiFeOx with overpotential in the range of 320–370 mV can be obtained for a wide range of Ni:Fe ratio[22] (**Table 1**). Noteworthy, the distribution of Ni and Fe along the thickness of the NiFeOx layer is not constant, therefore fixed Ni:Fe ratio from bulk

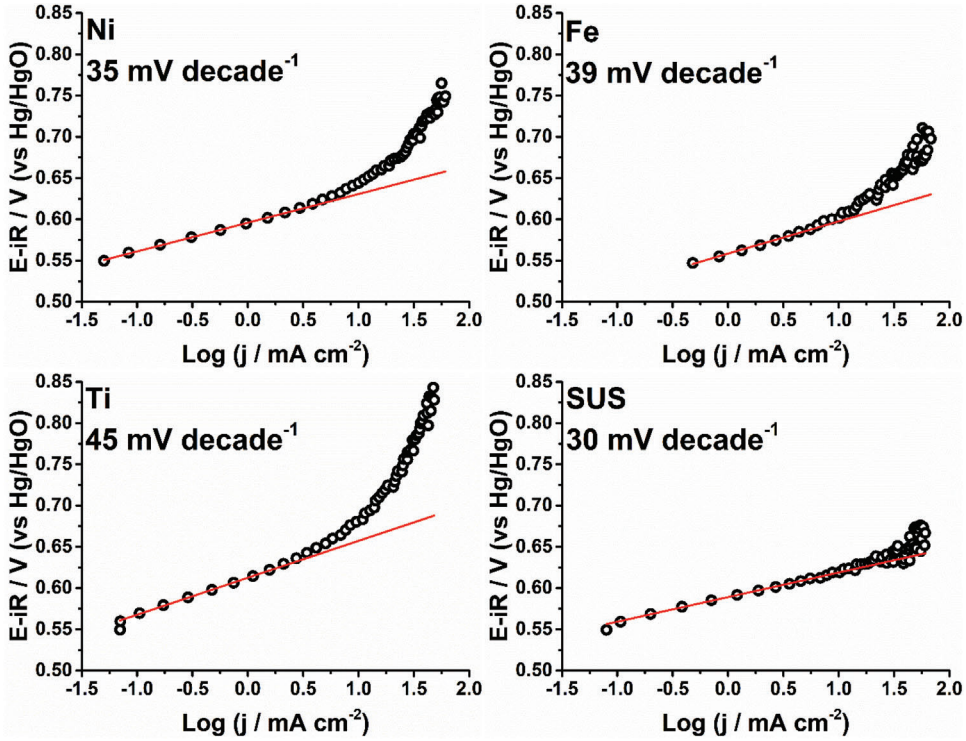

Figure 2. Tafel plot of NiFeOx deposited on Ni, Fe, Ti, and SUS in 1 M NaOH. Quasi steady-state polarization: step of 10 mV and 60 s.

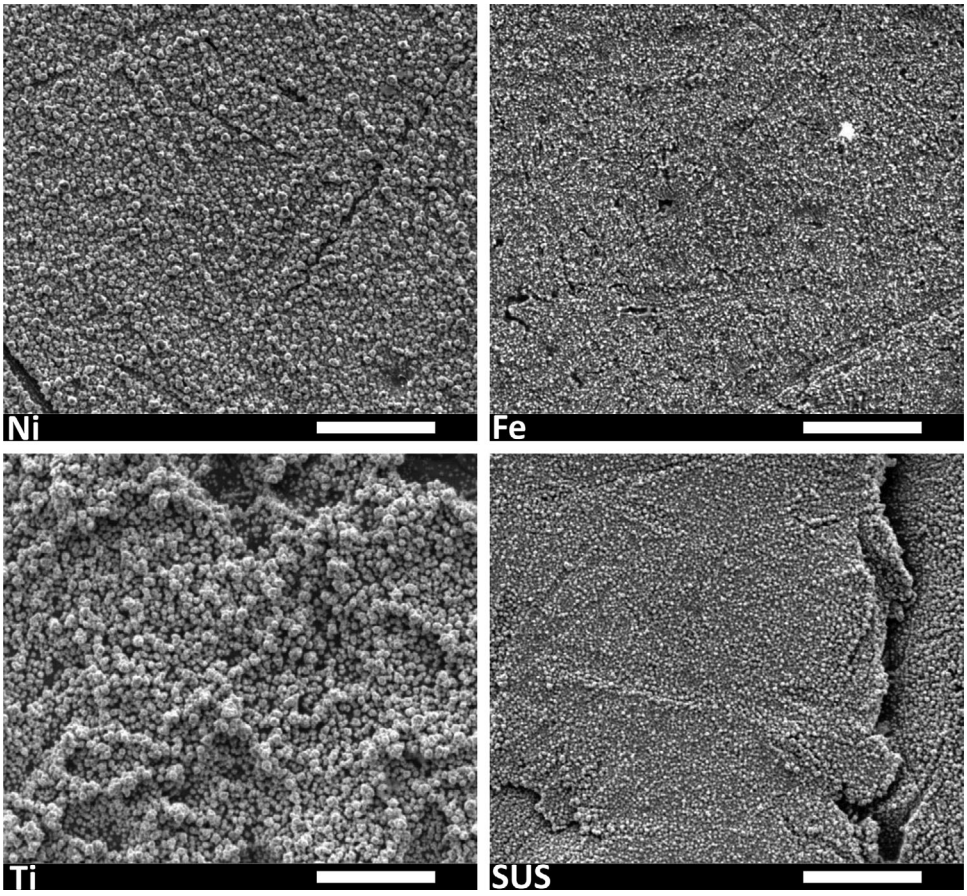

Figure 3. SEM micrographs of NiFeOx deposited on Ni, Fe, Ti, and SUS. Scale bar: 5 μm.

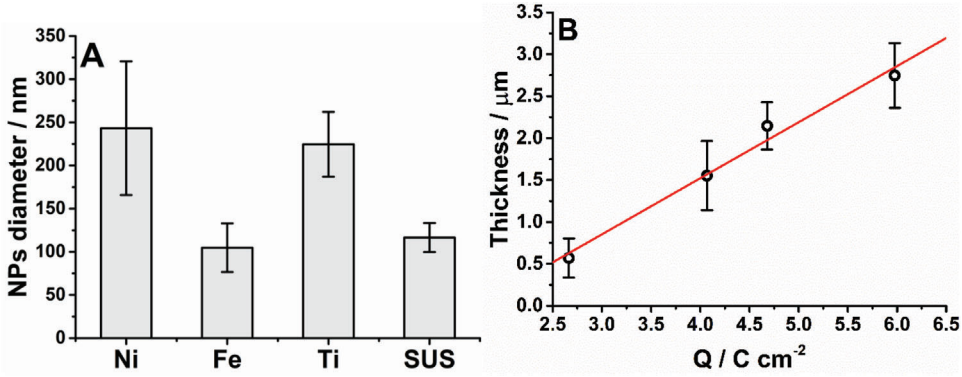

Figure 4. NiFeOx NPs diameter A), and correlation between thickness and total charge used in the electrodeposition B).

analysis, XPS surface analysis, or starting plating solution concentrations, do not represent adequately the heterogeneous deposition of the NiFeOx layer which is better described by depth profile analysis, as in the present case obtained from GDOES measurements.

From the previous characterizations, we assessed the good quality of the NiFeOx electrocatalyst, as our values are comparable to those available in the literature,[17–20,22–24,39] thus confirming the state-of-the-art activity for the WOR (Table 1). In particular, by electrodeposition optimization, we proved that the four substrates did not affect the intrinsic properties of the NiFeOx in terms of overpotential and Tafel slope, and in principle, all could be suitable for the fabrication of an electrode. The effect of the substrate is although evident on the electrodeposition process because the optimal NiFeOx layer is prepared at different reduction potential and time resulting in different nanoparticles size and layer thickness (Figure 4).

To assess which substrate would be more suitable, WOR stability tests were conducted by continuous galvanostatic electrolysis. The stability has been evaluated by potential variation from the start and conclusion of the chronopotentiogram (**Figure 5**).

Stainless steel showed the highest stability among the four substrates, in combination with the lowest overpotential. The ΔE was (SUS) 8 mV < (Ni) 23 mV < (Fe) 27 mV < (Ti) 54 mV.

Also in case of cycling (1 h × 5 times), stainless steel was superior to all other substrates (**Figure 6**; Figure S10, Supporting Information). In particular, we noticed that the starting potential is recovered at the beginning of the next galvanostatic cycle (Figure S11, Supporting Information).

Table 1. Summary of NiFeOx electrochemical and physical characteristics for the substrate material.

	Ni	Fe	Ti	SUS
η / mV	342	324	374	325
Tafel / mV dec^{-1}	35	39	45	30
NPs / nm	243 ± 77	105 ± 28	225 ± 38	117 ± 17
Thickness / µm	1.6 ± 0.4	2.1 ± 0.3	2.7 ± 0.4	0.6 ± 0.2
Fe % (surface)[a)]	20	17	17	4
Fe % (bulk)[a)]	19	91	21	62

[a)] Ni:Fe ratio details are available in Figures S8 and S9 (Supporting Information).

Qualitative XPS analysis, before and after the stability test, revealed limited changes on Fe oxidation state with slight increase of Fe(III), as most of the oxide is compatible with Fe_3O_4 and Fe_2O_3 (Figure S12, Supporting Information).[40,22] Ni showed a larger variation, with mainly NiO and Ni_2O_3 before, and $Ni(OH)_2$ after oxygen evolution reaction (Figure S13, Supporting Information).[41,22]

Morphological changes in the NiFe oxide nanoparticles, which can induce activity loss of the electrocatalyst,[42] have been evaluated by SEM imaging. Significant modifications were not observed as the nanoparticles diameter remained constant before and after the stability test (Figures S14 and S15, Supporting Information).

3. Conclusion

The electrocatalyst NiFeOx was deposited on 4 different metal substrates, namely nickel, iron, titanium and stainless steel, and used for the water oxidation reaction in alkaline conditions to assess the possibility of fabricating an electrode, and its stability based on the suitable substrate/electrocatalyst couple. The effect of the substrate material was evident in the electrodeposition process which affected the optimal potential and time of electrode-

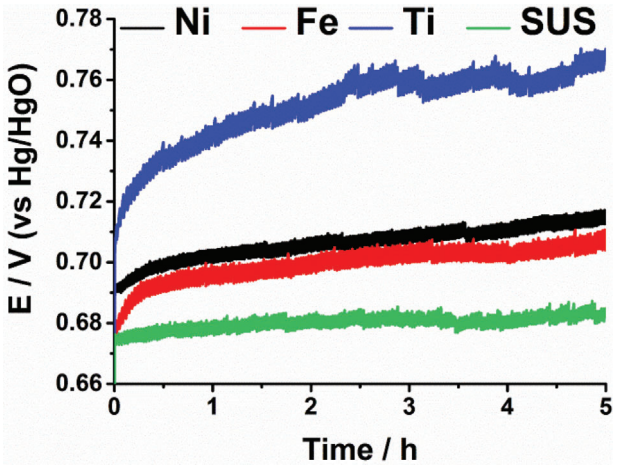

Figure 5. Potential variation for continuous galvanostatic electrolysis at 10 mA cm^{-2} in 1 M NaOH.

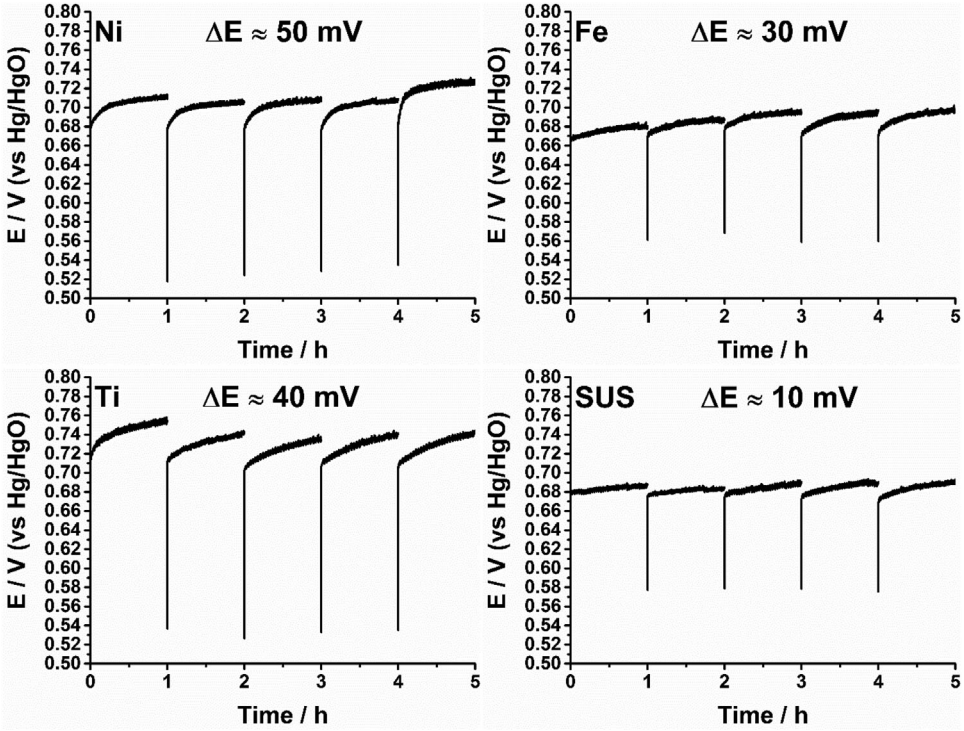

Figure 6. Potential variation for 5 cycles of 1 h by galvanostatic electrolysis at 10 mA cm^{-2} in 1 M NaOH.

position to obtain the best performing NiFeOx layer. In fact, the NiFeOx thickness and NPs diameter depends on the substrate. However, once the NiFeOx layer is formed, the nature of the substrate had a limited effect on the intrinsic properties of the NiFeOx, such as overpotential and Tafel slope, as they were similar and at the state-of-the-art. During galvanostatic electrolysis, the oxidation state of Fe shifts slightly from Fe(II) to Fe(III), likely Fe_3O_4 and Fe_2O_3, while NiO/Ni_2O_3 changed partially to $Ni(OH)_2$. Stability tests under galvanostatic conditions revealed stainless steel as the most suitable among the four substrates, with the lowest overpotential and highest potential stability. This result could be the effect of smaller NiFeOx nanoparticles compared to other substrates.

4. Experimental Section

Materials and Chemicals: Nickel, iron, stainless steel (SUS302), and titanium sheets (all thickness 0.5 mm) were purchased from Nilaco Co. (Japan). Nickel sulphate ($NiSO_4 \bullet 6H_2O$, ≥99.99%), iron sulphate ($FeSO_4 \bullet 7H_2O$, ≥99.0%), and ammonium sulphate ($(NH_4)_2SO_4$, ≥99.0%) were purchased from Sigma-Aldrich. Sodium hydroxide (NaOH, 97.0%) and isopropyl alcohol were purchased from Wako Pure Chemical Industries Ltd. (Japan).

Ultrapure water was produced from a Simply-Lab water system (DIRECT-Q 3 UV, Millipore) with a resistivity of 18.2 MΩ●cm at 25 °C.

Substrates Pretreatment: Ni, Fe, Ti, and SUS302 substrates were polished for 5 min with alumina sanding sponge (Microfine, 3 M Company). Ni, Fe, Ti and SUS302 were sonicated then in isopropyl alcohol and ultrapure water, for 5 min each. The Ti substrate was boiled for 1 h in 1 M oxalic acid, and finally rinsed with ultrapure water.[43]

Electrochemical Setup: Electrochemistry was conducted with a potentiostat PGSTAT302N (Metrohm). The PTFE electrochemical cell was a single-compartment with working electrode area delimited by a fluoroplatic O-ring (i.d. 16 mm), counter electrode was Pt spiral (l = 10 cm, d = 0.2 mm), and reference electrode was Hg/HgO (1 M NaOH). Conversion versus RHE is calculated by Equation (1) with $E^0_{Hg/HgO}$ (1 M NaOH) = 118 mV (vs NHE).

$$E_{RHE} = E_{Hg/HgO}\,(1M\ NaOH) + 0.0592 \times pH + E^0_{Hg/HgO}\,(1\ M\ NaOH) \quad (1)$$

For the NiFeOx electrodeposition only, the reference electrode was Ag/AgCl (KCl saturated).

Generally, all potentials are referred to the Hg/HgO (1 M NaOH) electrode, if not otherwise stated.

NiFeOx Electrodeposition Conditions: NiFeOx electrocatalyst was deposited on the substrate by chronoaperometry with optimization of applied potential and time (Figures S1–S3 and Table S1, Supporting Information) in a solution of 10 mM $NiSO_4$, 10 mM $FeSO_4$ and 20 mM $(NH_4)_2SO_4$ with pH adjusted to 3 by sulfuric acid.[20,22]

Characterizations: The surface of the electrodes was imaged by SEM (JCM-6000, JEOL, Tokyo, Japan), and NiFeOx layer thickness probed by DektakXT stylus profilometer (Bruker). The NiFeOx composition was analyzed by GDOES.[44] Electrochemical impedance spectroscopy (EIS) was conducted by ModuLabXM ECS (Solartron Analytical, Farnborough, U.K.) with an amplitude of 10 mV in the frequency range from 1 MHz to 100 mHz at open circuit potential.

Supporting Information

Supporting Information is available from the Wiley Online Library or from the author.

Acknowledgements

This work was partially supported by Grant-in-Aid for Scientific Research A 23H00288 (to Y.E.).

Conflict of Interest

The authors declare no conflict of interest.

Data Availability Statement

The data that support the findings of this study are available on request from the corresponding author. The data are not publicly available due to privacy or ethical restrictions.

Keywords

electrocatalyst, iron oxide, nickel oxide, stainless steel, Tafel, titanium, water oxidation reaction

Received: October 3, 2023
Revised: February 7, 2024
Published online: March 2, 2024

[1] N. Tanbouza, T. Ollevier, K. Lam, *iScience* **2020**, *23*, 101720.
[2] I. Moussallem, U. Kunz, P. Sinnow, T. Turek, *J. Appl. Electrochem.* **2008**, *38*, 1177.
[3] J. C. Ehlers, A. A. Feidenhans'l, K. T. Therkildsen, G. O. Larrazába, *ACS Energy Lett.* **2023**, *8*, 1502.
[4] A. Gawel, T. Jaster, D. Siegmund, J. Holzmann, H. Lohmann, E. Klemm, U.-P. Apfel, *iScience* **2022**, *25*, 104011.
[5] G. Qing, R. Ghazfar, S. T. Jackowski, F. Habibzadeh, M. M. Ashtiani, C.-P. Chen, M. R. Smith III, T. W. Hamann, *Chem. Rev.* **2020**, *120*, 5437.
[6] I. Katsounaros, *Curr. Opin. Electrochem.* **2021**, *28*, 100721.
[7] M. Breiner, M. Zirbes, S. R. Waldvogel, *Greeen Chem.* **2021**, *23*, 6449.
[8] S. Arndt, P. J. Kohlpaintner, K. Donsbach, S. R. Waldvogel, *Org. Process Res. Dev.* **2022**, *26*, 2564.
[9] J. Lee, J. H. Bang, *ACS Energy Lett.* **2020**, *5*, 2706.
[10] D. E. Danly, *J. Electrochem. Soc.* **1984**, *131*, 435C.
[11] Á. Vass, A. Kormányos, Z. Kószó, B. Endrődi, C. Janáky, *ACS Catal.* **2022**, *12*, 1037.
[12] M. Chatenet, B. G. Pollet, D. R. Dekel, F. Dionigi, J. Deseure, P. Millet, R. D. Braatz, M. Z. Bazant, M. Eikerling, I. Staffell, P. Balcombe, Y. Shao-Horn, H. Schäfer, *Chem. Soc. Rev.* **2022**, *51*, 4583.
[13] T. Reier, M. Oezaslan, P. Strasser, *ACS Catal.* **2012**, *2*, 1765.
[14] S. Trasatti, G. Buzzanca, *J. Electroanal. Chem.* **1971**, *29*, A1.
[15] S. Park, Y. H. Lee, S. Choi, H. Seo, M. Y. Lee, M. Balamurugan, K. T. Nam, *Energy Environ. Sci.* **2020**, *13*, 2310.
[16] N. Comisso, L. Armelao, S. Cattarin, S. Fasolin, L. Mattarozzi, M. Musiani, M. Rancan, L. Vázquez-Gómez, E. Verlato, *J. Electroanal. Chem.* **2021**, *880*, 114844.
[17] C. C. L. McCrory, S. Jung, J. C. Peters, T. F. Jaramillo, *J. Am. Chem. Soc.* **2013**, *135*, 16977.
[18] D. A. Corrigan, *J. Electrochem. Soc.* **1987**, *134*, 377.
[19] E. Potvin, L. Brossard, *Mater. Chem. Phys.* **1992**, *31*, 311.
[20] M. D. Merrill, R. C. Dougherty, *J. Phys. Chem. C* **2008**, *112*, 3655.
[21] K. H. Kim, J. Y. Zheng, W. Shin, Y. S. Kang, *RSC Adv.* **2012**, *2*, 4759.
[22] M. W. Louie, A. T. Bell, *J. Am. Chem. Soc.* **2013**, *135*, 12329.
[23] L. Bai, S. Lee, X. Hu, *Angew. Chem., Int. Ed.* **2021**, *60*, 3095.
[24] A. Sakamaki, M. Yoshida-Hirahara, H. Ogihara, H. Kurokawa, *Langmuir* **2022**, *38*, 5525.
[25] S. Trasatti, *Electrochim. Acta* **2000**, *45*, 2377.
[26] S. Trasatti, *Electrochim. Acta* **1991**, *36*, 225.
[27] P. Duby, *JOM* **1993**, *45*, 41.
[28] D. Baronetto, I. M. Kodintsev, S. Trasatti, *J. Appl. Electrochem.* **1994**, *24*, 189.
[29] E. Mahé, D. Devilliers, *Electrochim. Acta* **2000**, *46*, 629.
[30] T. Reier, D. Teschner, T. Lunkenbein, A. Bergmann, S. Selve, R. Kraehnert, R. Schlögl, P. Strasser, *J. Electrochem. Soc.* **2014**, *161*, F876.
[31] F. Dionigi, P. Strasser, *Adv. Energy Mater.* **2016**, *6*, 1600621.
[32] X. Deng, D. C. Sorescu, I. Waluyo, A. Hunt, D. R. Kauffman, *ACS Catal.* **2020**, *10*, 11768.
[33] N. Todoroki, T. Wadayama, *ACS Appl. Mater. Interfaces* **2019**, *11*, 44161.
[34] Y. K. Kim, W. T. Jun, D. H. Youn, J. S. Lee, *J. Alloys Compd.* **2022**, *901*, 163689.
[35] V. Krstić, B. Pešovski, *Hydrometallurgy* **2019**, *185*, 71.
[36] C. Gütz, A. Stenglein, S. R. Waldvogel, *Org. Process Res. Dev.* **2017**, *21*, 771.
[37] A. Damjanovic, A. Dey, J. O.'M. Bockris, *Electrochim. Acta* **1966**, *11*, 791.
[38] Y.-H. Fang, Z.-P. Liu, *ACS Catal.* **2014**, *4*, 4364.
[39] F. Song, M. M. Busch, B. Lassalle-Kaiser, C.-S. Hsu, E. Petkucheva, M. Bensimon, H. M. Chen, C. Corminboeuf, X. Hu, *ACS Cent. Sci.* **2019**, *5*, 558.
[40] T. Yamashita, P. Hayes, *Appl. Surf. Sci.* **2008**, *254*, 2441.
[41] A. Davidson, J. F. Tempere, M. Che, H. Roulet, G. Dufour, *J. Phys. Chem.* **1996**, *100*, 4919.
[42] F.-M. Li, L. Huang, S. Zaman, W. Guo, H. Liu, X. Guo, B. Y. Xia, *Adv. Mater.* **2022**, *34*, 2200840.
[43] C. H. Angell, (Imperial Chemical Industries Ltd), USA US3650861A, **1972**.
[44] A. Vesel, R. Zaplotnik, G. Primc, M. Mozetic, *J. Vac. Sci. Technol. A* **2023**, *41*, 040801.